



Article

Feasibility Assessment of Hydrophobic Surface Creation via Digital Light Processing: Influence of Texture Geometry, Composition, and Resin Type

Saher Mohammed Abo Shawish, Mohsen Barmouz * and Bahman Azarhoushang

Institute for Advanced Manufacturing (KSF), Furtwangen University, 78532 Tuttlingen, Germany; sahermohammeda@gmail.com (S.M.A.S.); bahman.azarhoushang@hs-furtwangen.de (B.A.)

* Correspondence: mohsen.barmouz@hs-furtwangen.de

Abstract

This study explores the fabrication of hydrophobic surfaces on polymer components via Digital Light Processing (DLP), with emphases on how texture geometry, feature dimensions, and resin type influence surface wettability. Square and cylindrical microtextures were fabricated and evaluated using static contact angle measurements. Square-shaped structures demonstrated enhanced hydrophobicity, with contact angles reaching 133.6°, compared to approximately 100° for cylindrical counterparts of identical dimensions. Increasing pillar height to 521 μm enhanced hydrophobicity by approximately 15%, while decreasing pillar spacing to 150 μm increased contact angles from 86.8° to 106°, highlighting the role of microstructure density. For square-shaped structures, the addition of a hydrophobic agent at 3 wt.% resulted in a contact angle of 123.4°, representing a 44% improvement over the untreated sample. These findings underscore the combined influence of resin chemistry, surface texture design, and dimensional parameters on wettability behavior. Although superhydrophobicity (contact angle > 150°) was not achieved, the study demonstrates notable advancements in optimizing hydrophobicity through DLP printing. Overall, the results support DLP as a scalable and cost-effective approach for engineering functional surfaces suited to self-cleaning, biomedical, and anti-fouling applications.



Academic Editor: Jiunn Jer Hwang

Received: 14 July 2025

Revised: 11 August 2025

Accepted: 13 August 2025

Published: 19 August 2025

Citation: Abo Shawish, S.M.; Barmouz, M.; Azarhoushang, B. Feasibility Assessment of Hydrophobic Surface Creation via Digital Light Processing: Influence of Texture Geometry, Composition, and Resin Type. *J. Compos. Sci.* **2025**, *9*, 447. <https://doi.org/10.3390/jcs9080447>

Copyright: © 2025 by the authors. Licensee MDPI, Basel, Switzerland. This article is an open access article distributed under the terms and conditions of the Creative Commons Attribution (CC BY) license (<https://creativecommons.org/licenses/by/4.0/>).

Keywords: hydrophobic surfaces; digital light processing (DLP); additive manufacturing; texture geometry; contact angle; surface engineering; photopolymer resins; superhydrophobicity; surface wettability

1. Introduction

Hydrophobic and superhydrophobic (SHB) surfaces have garnered increasing interest due to their relevance in diverse applications, including those relating to drag reduction, self-cleaning, microfluidics, and corrosion resistance [1]. Hydrophobicity is typically defined by a water contact angle (WCA) of above 90°, while SHB surfaces exhibit WCA values above 150° with low roll-off angles, which facilitate droplet mobility [2]. This behavior is largely attributed to micro/nanostructures coupled with low-surface-energy materials—a phenomenon commonly referred to as the ‘lotus effect’ [3,4]. SHB coatings have been widely explored in the contexts of biomedical devices, microfluidics, heat exchangers, and anti-fouling surfaces. For example, their anti-icing properties significantly reduce ice adhesion, enhancing performance in cold environments [5]. In biomedical applications, superhydrophobic coatings minimize blood adhesion and cell attachment, thereby reducing complications related to thrombosis [1,6,7]. They enhance blood compatibility, reduce

bacterial adhesion, and improve heat transfer efficiency by forming an air barrier that inhibits protein anchoring and influences cellular behaviors such as adhesion, morphology, and proliferation [8–10]. Moreover, superhydrophobic surfaces have shown effectiveness in preventing bacterial adhesion on medical implants, which lowers infection risks while maintaining biocompatibility [11–13]. In microfluidic devices, SHB surfaces reduce drag and improve fluid transport efficiency. Kang et al. (2023) highlighted the role of precision in 3D printing in achieving consistent hydrophobicity across complex microchannels [14]. Industrial applications benefit from SHB surfaces through enhanced anti-corrosion and anti-icing performance, drag reduction in watercraft, and improved evaporation and condensation efficiency. These advantages stem from the extreme wetting characteristics of these surfaces, particularly the water contact angles exceeding 150° and sliding angles below 10° . These allow droplets to bead up and roll off easily, minimizing surface contamination and liquid adhesion. The trapped air within their micro/nanostructures further prevents direct contact between liquids and the underlying material, providing additional protection [15]. In machining, durable SHB steel has proven effective in withstanding harsh industrial conditions and preventing corrosion [16]. SHB coatings contribute to efficient thermal management in heat exchangers by promoting effective boiling and condensation [17]. They also enhance slip resistance in watercraft by reducing drag and preventing biofouling. This not only improves fuel efficiency but also reduces maintenance by preventing the accumulation of marine organisms and biofilms [15]. Self-cleaning applications, widely used in coatings and textiles, benefit from SHB-inspired microtextures that facilitate dirt removal and maintain cleanliness [18–20]. The development of pillar arrays and hierarchical structures through Digital Light Processing (DLP) 3D printing has proven effective in enhancing self-cleaning performance by reducing water contact and promoting roll-off behavior [21]. However, conventional fabrication methods are often associated with high costs, limited scalability, inconsistent results, and challenges in applying coatings to complex geometries [22]. In contrast, Digital Light Processing (DLP), a subset of vat photopolymerization, offers a promising alternative due to its design flexibility, high resolution, and reduced material waste. It enables the efficient fabrication of lightweight, high-strength components for diverse applications [23–27]. Furthermore, DLP's user-friendliness makes it accessible to a broader range of users, including those with limited technical expertise [24]. This positions DLP as an ideal candidate for fabricating tailored, high-performance hydrophobic surfaces efficiently and reliably. Although previous studies, such as those by Kaur et al. (2020) [21] and Han et al. (2018) [28], have successfully demonstrated the fabrication of hydrophobic surfaces using DLP by integrating hydrophobic additives and microtexture-based designs, their investigations lacked a systematic evaluation of texture geometry. This study addresses these limitations by experimentally analyzing the combined effects of surface shape (cylindrical and square) and dimensional parameters (height, spacing, and base width) on contact angle performance—an area not comprehensively explored in previous research.

Moreover, the inclusion of commercial resin types adds a new comparative dimension to hydrophobic material selection. Earlier works often employed customized resins, which limits practical applicability and reproducibility. In contrast, commercial resins contain hydrophilic agents, thereby increasing the difficulty of achieving hydrophobic performance; their use in this study enhances the practical relevance of the experimental design by reflecting real-world application conditions. By addressing both geometric and material variables within a unified experimental framework, this study fills a critical gap in understanding the governing factors of wettability in DLP-fabricated polymeric surfaces.

This study aims to evaluate the feasibility of using DLP to fabricate hydrophobic polymer surfaces by optimizing texture geometry and printing parameters, with the ultimate

goal of producing durable, functional surfaces exhibiting high contact angles, low roll-off behavior, and environmental stability.

Fundamentals of Surface Wettability

Wetting is a common natural phenomenon that many organisms exploit for survival [29,30]. For example, lotus leaves exhibit self-cleaning abilities, water striders walk on water, and spider silk and the Namib Desert beetle collect water efficiently [29,31,32]. Engineered control of wetting behavior enables applications involving heat transfer, microfluidics, anti-corrosion, and anti-fouling surfaces [29]. Despite significant research, the complex mechanisms of wetting, particularly at different scales, are not fully understood [29]. Advances in micro- and nanofabrication technologies, following Wenzel’s discovery of the link between roughness and wettability [33], have enabled the precise design of hydrophilic and hydrophobic surfaces [34]. On rough surfaces, droplets can fully wet the texture (Wenzel state) or partially wet it while trapping air (Cassie–Baxter state) [29], as illustrated in Figure 1. Moreover, understanding wetting at elevated temperatures (30–90 °C) is critical for applications like water transport and metal processing, in which surface quality influences boiling, heat exchange, and drying [35,36].

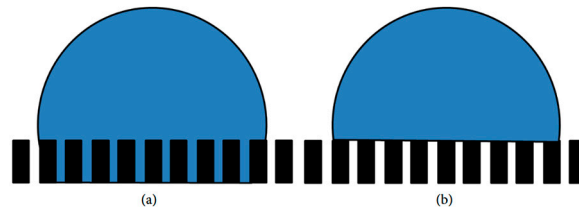


Figure 1. (a) The Wenzel state and (b) droplets on a microstructured surface in the Wenzel state [29].

One widely used method to quantify surface wettability is through contact angle measurements, where a small droplet of liquid is placed on a surface and its shape is analyzed [4]. Young’s equation relates the interfacial energies to the contact angle on a smooth surface (Figure 2, top center) [37].

$$\cos\theta = (\gamma_{SV} - \gamma_{SL})/\gamma_{LV} \tag{1}$$

where

- γ_{SV} is the solid–vapor interfacial tension;
- γ_{SL} is the solid–liquid interfacial tension;
- γ_{LV} is the liquid–vapor interfacial tension.

Surface roughness alters the wetting behavior; when the droplet fully penetrates the grooves, the Wenzel model applies:

$$\cos\theta_\omega = r \cos\theta \tag{2}$$

where $r (>1)$ is the roughness factor, representing the ratio of actual to projected surface area [6]. If air pockets remain trapped beneath the droplet, forming a composite solid–air interface, the Cassie–Baxter model applies (Figure 2, bottom left B) [38].

$$\cos\theta_{CB} = f_1 \cos\theta_1 + f_2 \cos\theta_2 \tag{3}$$

With $\theta_2 = 180^\circ$ and $f_1 + f_2 = 1$, this can be simplified to

$$\cos\theta_{CB} = f_1 (\cos\theta_1 + 1) - 1 \tag{4}$$

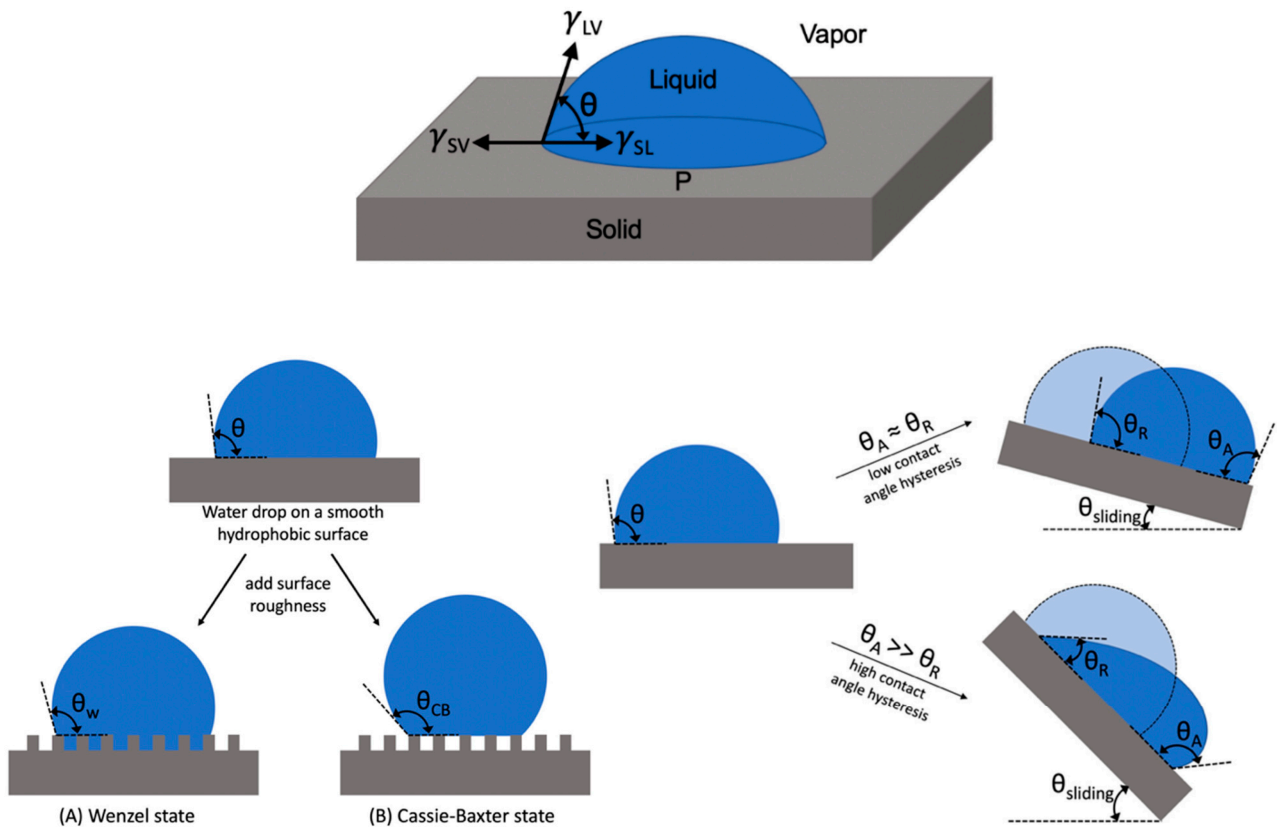


Figure 2. Schematic representation of hydrophobicity and wetting states: The (top center) shows Young’s equation for a liquid drop on a smooth, solid surface. The (bottom left) subfigures (A) Wenzel state and (B) Cassie–Baxter state illustrates how surface roughness increases the contact angle, as described by the Wenzel and Cassie–Baxter models. The (bottom right) shows contact angle hysteresis and droplet sliding on a tilted surface, with advancing (θ_A) and receding (θ_R) angles and sliding behavior [4].

Because $f_1 < 1$, the apparent contact angle exceeds that of a smooth surface, as exemplified by the lotus leaf effect. These models explain the hydrophobicity of flat, stationary surfaces. However, even on hydrophobic or superhydrophobic surfaces, water droplets may adhere and not roll off when the surface is tilted, a phenomenon quantified by contact angle hysteresis (CAH), the difference between advancing θ_A and receding θ_R angles, as shown in Figure 2, “Schematic representation of hydrophobicity and wetting states”. The top center shows Young’s equation for a liquid drop on a smooth solid surface. The bottom left illustrates how surface roughness increases the contact angle, as described by the Wenzel and Cassie–Baxter models. The bottom right shows contact angle hysteresis and droplet sliding on a tilted surface, with advancing (θ_A) and receding (θ_R) angles and sliding behavior [4].

Many researchers attribute CAH to an imbalance at the liquid–solid interface [6]. Factors such as the velocity of the three-phase contact line, surface roughness, chemical stickiness, and the interactions between the water and air molecules and the solid surface all influence CAH [38]. The force F required to move a liquid droplet over a flat solid surface can be expressed as

$$F = \gamma LV Rk (\cos\theta_R + \cos\theta_A) \tag{5}$$

where R is the droplet radius, k is a shape-dependent constant, and γLV is the liquid–vapor surface tension; this force must overcome the droplet’s gravitational component, given

by $mg \sin \alpha$, where m is the droplet mass and α is the surface tilt angle. As Equation (5) indicates, higher CAH increases the critical force required to initiate droplet motion. Water-repellent surfaces are characterized by low CAH. When a surface exhibits a high water contact angle ($WCA > 150^\circ$) and low CAH, indicating minimal solid–liquid adhesion (SA), the surface is termed superhydrophobic [4].

2. Materials and Methods

This study aimed to fabricate hydrophobic surfaces using Digital Light Processing (DLP) technology by selecting suitable materials, designing microstructures, and optimizing printing parameters. Three commercially available photopolymer resins were utilized: TR300 Ultra-High Temp Resin (Phrozen, 3F, No. 287, Niupu Rd., Xiangshan District, Hsinchu City, Taiwan), Speed Resin (Phrozen, Hsinchu City, Taiwan), and Water-Washable Dental Model Resin (Phrozen, Hsinchu City, Taiwan). These resins were selected based on viscosity, mechanical strength, and surface energy, factors that influence both DLP compatibility and hydrophobic performance. The TR300 resin is known for its high heat resistance, with a heat deflection temperature of 160°C , and its mechanical strength is suitable for the durable, high-performance components used in elevated thermal conditions [39]. The Speed resin offers rapid printing capabilities, up to 8 times faster than those of conventional resins, and supports large model production (up to 24 cm in height) within 6 h, making it sufficiently versatile for prototypes and cosplay props [40]. The Water-Washable Dental Model Resin provides high precision with an accuracy of ± 0.05 mm; features water-washable post-processing, eliminating the need for solvents such as ethanol or isopropanol; and has low levels of shrinkage and odor, enhancing user experience and suitability with respect to fine surface details [41]. Among the three, the Water-Washable resin demonstrated the best performance in terms of dimensional precision and solvent-free post-processing, making it particularly suitable for applications requiring fine surface details. Its superior hydrophobic performance is likely due to its balanced surface tension and chemical formulation, which may reduce polar interactions at the interface. To prevent the sedimentation of additives and ensure stable dispersion, hydrophobic fumed silica (commercially labeled as Pyrogenie Kieselsäure Hydrophob, supplied by Thielcoating, Germany) was added to the resin mixtures in concentrations of 1%, 2%, 3%, and 4% by weight. The fumed silica also acted as an anti-settling agent and promoted uniform particle distribution by forming a hydrophobic barrier that counteracted gravitational separation within the resin matrix. The mixing protocol included two steps: initial manual stirring to pre-disperse the silica, followed by mechanical mixing using a laboratory overhead stirrer (Steinberg Systems, model SBS-EB-1000, Poland) at 500 RPM for 2–5 min, depending on the resin's viscosity, with higher-viscosity resins requiring longer mixing durations to ensure homogeneity. Following material preparation, two types of surface microstructures were designed to assess the influence of geometry on water repellency. Arrays of square pillars with variable dimensions—side length (x), spacing (y), and height (z)—were fabricated on flat and 3D surfaces, as illustrated in Figure 3 (top left). Feature widths ranged from 150 to 600 μm , with heights and spacings between 200 and 500 μm . Square pillar designs were inspired by the Cassie–Baxter wetting state found in nature and modeled after lotus leaf structures known for their self-cleaning properties [21]. Cylindrical pillars, as seen in Figure 3 (top right), were modeled based on perfluoropolyether-based designs, as reported in the literature, that demonstrated effective repellency to water and oil, depending on texture roughness and spacing. All geometries were created using SolidWorks (Version 2022, Dassault Systèmes, Vélizy-Villacoublay, France) with parametric design tools utilized to precisely control height, spacing, and texture density Figure 3. The 3D models were then sliced using ChituBox (Version 3.0.0, CBD-Tech, Shenzhen, China) and printing parameters

(layer thickness and exposure time) were adjusted to ensure high-resolution replication. Most samples were printed at layer thicknesses of 50 μm and 100 μm , while 25 μm was used for high-detail structures. Support structures were customized according to part orientation to minimize distortion during printing.

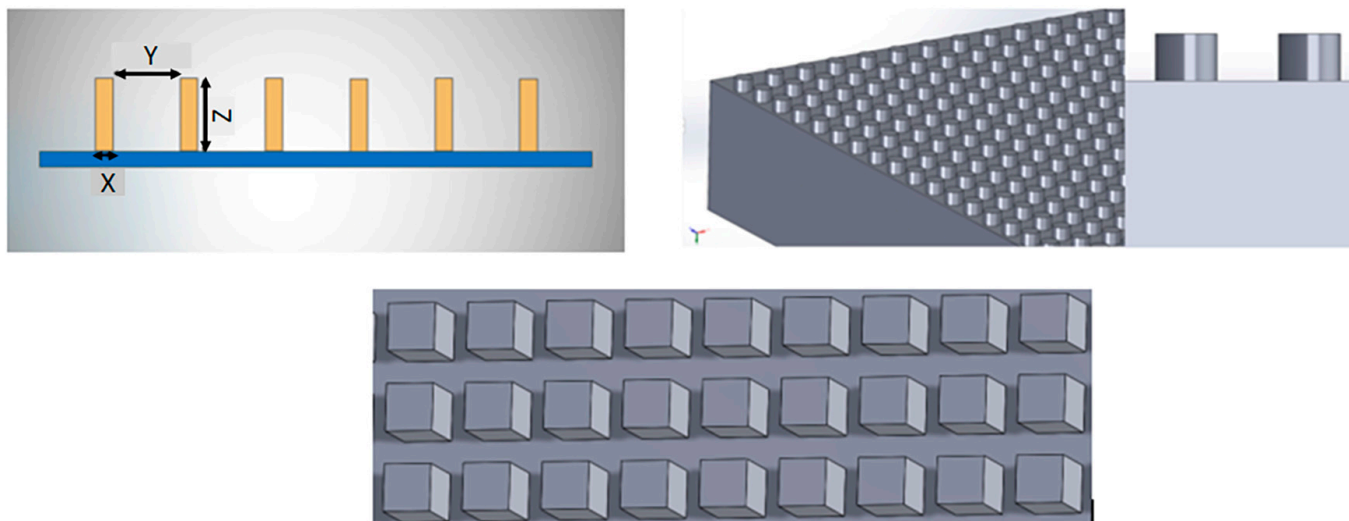


Figure 3. Geometrical and 3D representations of square and cylindrical pillar arrays. Top left: Illustration of the geometrical parameters of regular square pillars with labeled dimensions. Top right: 3D cylindrical model designed in SolidWorks. Bottom: 3D representation of the square pillar arrangement on the surface.

Fabrication was performed using a high-resolution DLP printer ((Phrozen Sonic Mighty 8K, Phrozen Tech., Hsinchu, Taiwan), which employs masked stereolithography (MSLA) with a pixel resolution of 28 μm and Z-axis accuracy of up to 10 μm . Post-processing involved cleaning the printed samples using a digital ultrasonic cleaner. Isopropyl alcohol was used for the TR300 and Speed resins, whereas deionized water was used for the Water-Washable resin. Surface characteristics were examined using a VHX-5000 digital microscope ((Keyence Corp., Osaka, Japan), offering magnifications up to 5000 \times , 3D surface imaging, and advanced texture analysis capabilities. Hydrophobicity was evaluated through static contact angle measurements by placing a 2 μL droplet of deionized water on the surface, with images then captured from multiple viewing angles using an optical goniometer (Krüss GmbH, Hamburg, Germany). Surfaces exhibiting contact angles above 90° were considered hydrophobic, while those exceeding 150° were classified as superhydrophobic, according to standard criteria [2]. The mean contact angle was calculated from repeated measurements to ensure reliability and reproducibility. Specifically, for each sample, contact angle measurements were taken at six different points (four corners and two center points), using three droplet measurements per location. The average contact angle and standard deviation were then calculated and reported to quantify measurement variability.

3. Results

3.1. Printing Accuracy Analysis

The microstructures of the fabricated surfaces were examined using a VHX Digital Microscope to assess surface roughness and structural uniformity Figure 4. The images show that both square and cylindrical shapes were successfully replicated, with minimal fabrication defects. Slight inconsistencies in pillar height and spacing were observed in the samples printed with shorter exposure times.

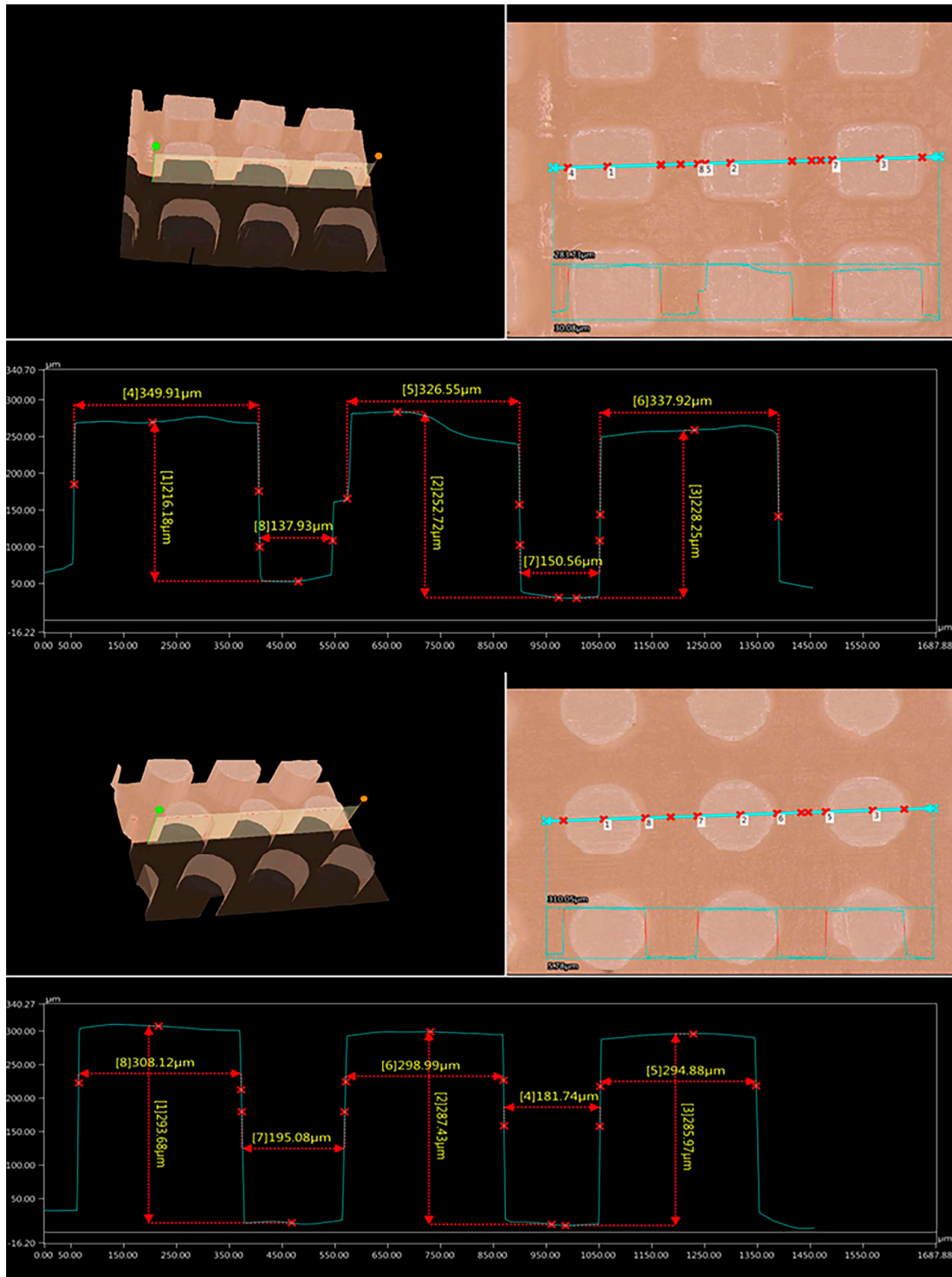


Figure 4. Square and cylindrical textures captured under the digital microscope, along with dimensional measurements.

3.2. The Effect of Resin Type

Figure 5 presents contact angle measurements for three pure resins: TR300, Speed, and Water-Washable. The Pure Water-Washable resin demonstrated the highest contact angle (90.3°), followed by Pure Speed (78.3°), and then Pure TR300 (71.7°). Compared to TR300, the Water-Washable resin showed an increase in hydrophobicity of approximately 26%, while Speed showed an increase of around 9.1%. These findings underscore the substantial

influence of resin chemistry on surface wettability, with the Water-Washable resin offering the most promising performance for hydrophobic surface fabrication.

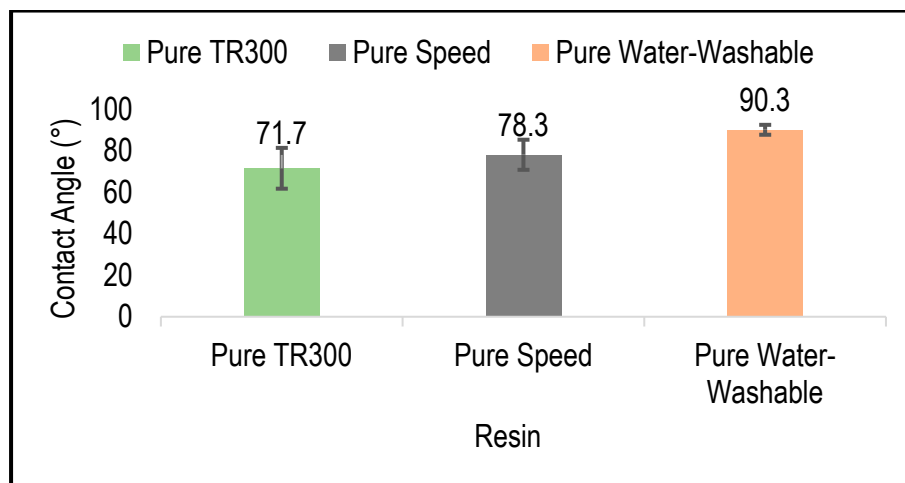


Figure 5. Measurements of contact angles for several resin varieties show the pure Water-Washable resin to have the maximum hydrophobicity.

3.3. The Effect of Geometry on Hydrophobicity

Following the identification of Water-Washable resin as the most hydrophobic material, the influence of surface geometry was examined. As shown in Figure 6, square-shaped microstructures consistently exhibited higher contact angles than cylindrical ones under all tested geometric configurations. For instance, in the 300 μm dimension (Dim) × 300 μm height (H) × 200 μm distance (dis) configuration, the square geometry achieved a contact angle of approximately 106.08°, while its cylindrical counterpart showed the lower value of 99.62°. This corresponds to a 6.5% increase in water repellency due to the square texture. This enhancement may be attributed to increased air entrapment and the more effective surface roughness created by the square microstructure.

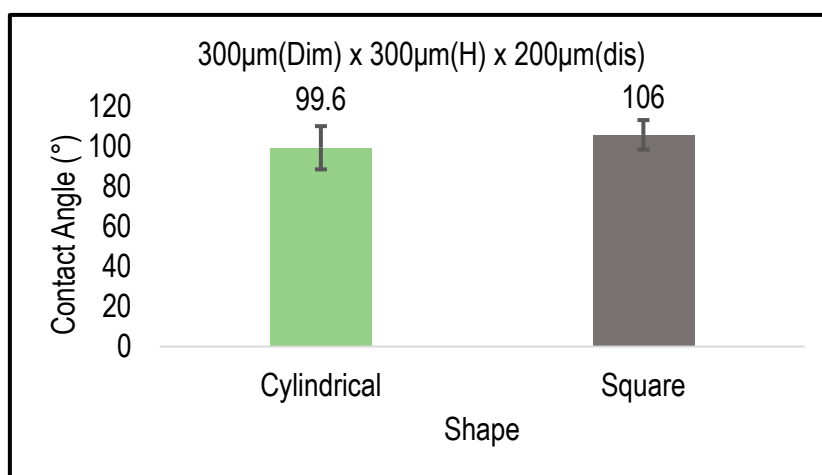


Figure 6. Comparison of 300 Dim × 300 H × 200 dis, square and cylindrical.

3.4. The Effects of Dimensions on Hydrophobicity

As shown in Figure 7, the data clearly demonstrate that increasing surface feature dimensions enhances hydrophobicity, for both the square and cylindrical textures. In the case of the square texture, the contact angle increased from 106.08° at 300 μm to 128.36° at 460 μm, corresponding to a 21.0% increase in water repellency. Similarly, cylindrical

textures also exhibited a significant increase: the contact angle rose from 77.5° at 200 μm to 99.6° at 300 μm, reflecting a 28.5% improvement. These enhancements are likely due to the increased surface roughness and air entrapment at larger feature sizes, which reduce the contact areas between the water droplets and the surface.

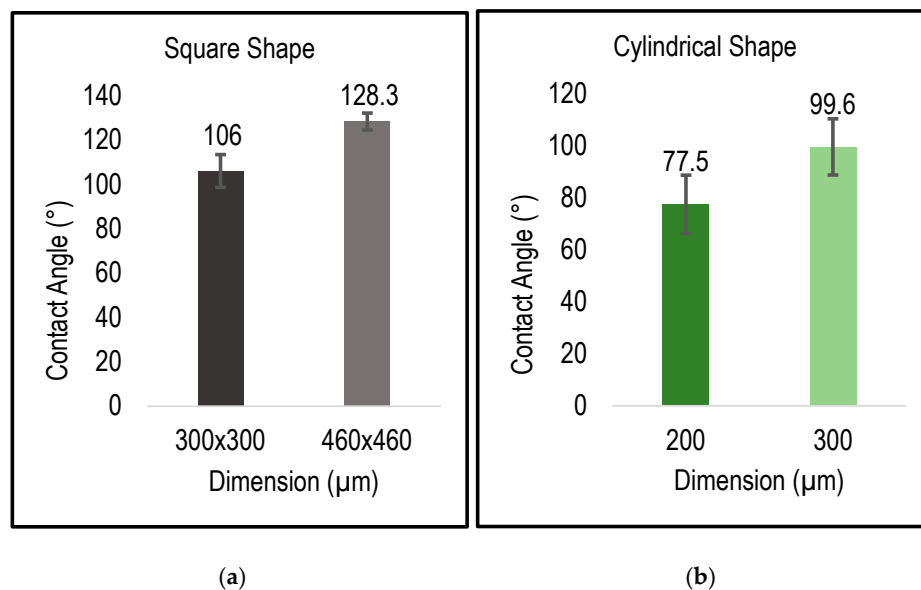


Figure 7. Influence of surface dimensions on hydrophobicity: (a) square textures; (b) cylindrical textures.

3.5. The Effect of Height

In this experiment, the surface area (510 × 510 μm) and spacing (150 μm) were kept constant to isolate the effect of pillar height on surface wettability. The results, described in Figure 8, show that increasing the pillar height from 350 μm to 521 μm led to an increase in contact angle from 116.4° to 133.6°. This corresponds to an approximate 14.8% improvement in hydrophobicity. The enhancement may be attributed to greater vertical roughness, which promotes air trapping and reduces the effective contact area between the droplet and the surface. Additionally, taller pillars support the stability of the Cassie–Baxter wetting state by minimizing liquid penetration into the texture, thereby enhancing water repellency and droplet mobility.

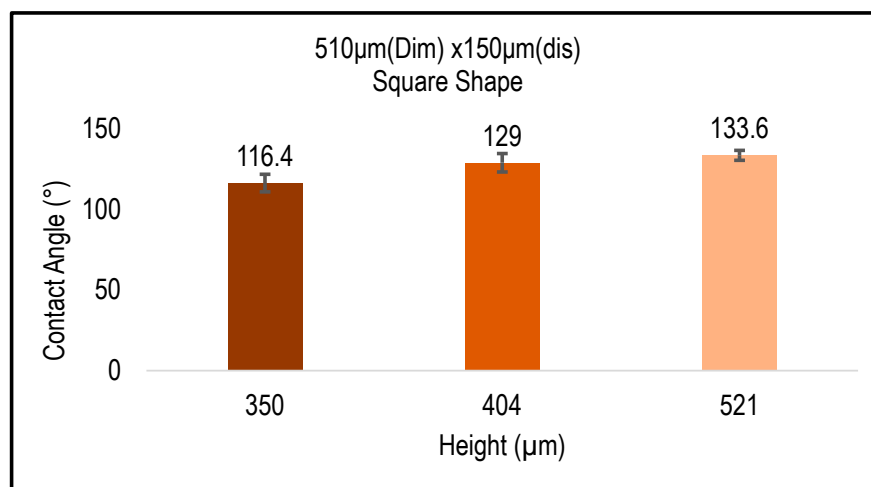


Figure 8. Effect of pillar height on the contact angle, for 510 × 510 μm square surfaces.

3.6. The Effect of Distance

Figure 9 shows that reducing the spacing distance between the microstructures results in increased contact angles, thereby enhancing hydrophobicity. For square-shaped textures, decreasing the spacing from 258 μm to 150 μm resulted in an increase in the contact angle from 86.84° to 106.08°, which corresponds to a 22.2% improvement. Similarly, for cylindrical textures, reducing the spacing from 303 μm to 195 μm led to an increase in the contact angle from 69.6° to 99.6°, indicating a significant 43.1% improvement. This effect is attributed to the denser arrangement of pillars, which increases air entrapment and reduces the effective solid–liquid contact area.

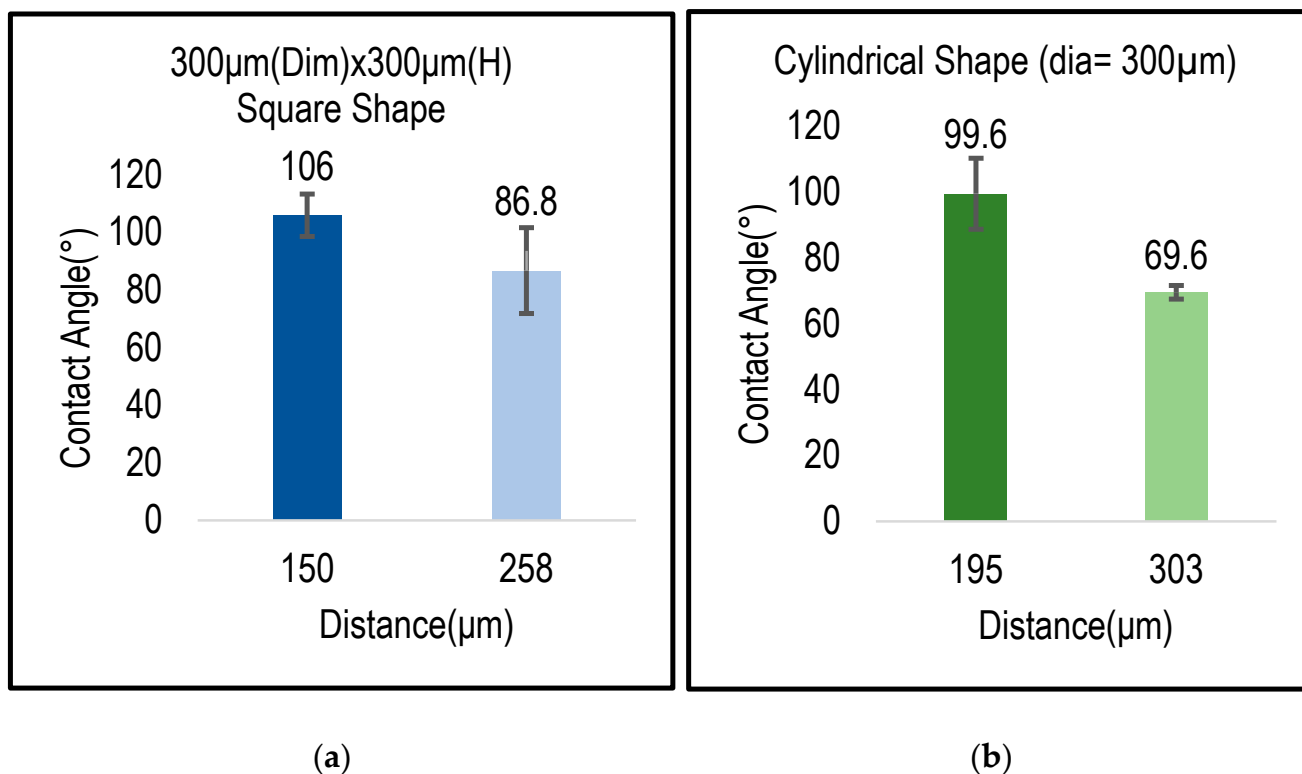


Figure 9. (a) Effect of spacing distance on contact angle for square; (b) effect of spacing distance on contact angle for cylindrical geometries.

3.7. Hydrophobic Agent Percentage

Figure 10 illustrates the effects of varying concentrations of the hydrophobic agent (HFS) on the contact angles of 510 \times 510 μm square-shaped structures. Introducing 1% HFS significantly increased the contact angle from 85.1° (without HFS) to 113.1°, corresponding to a 32.9% improvement in hydrophobicity. Increasing the concentration to 2% and 3% HFS resulted in enhancements that were more moderate, raising the contact angle to 120.4° and 123.4°, respectively, corresponding to 6.5% and 2.5% increases relative to the previous concentration. These results highlight the effectiveness of the hydrophobic agent in improving water repellency, with diminishing returns evident at higher concentrations.

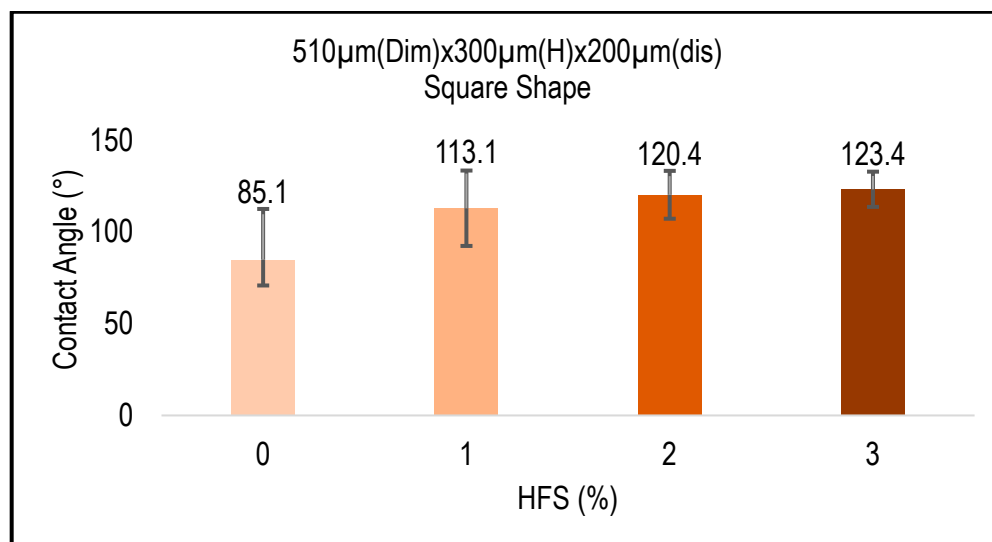


Figure 10. Effect of hydrophobic agent percentage on contact angle.

4. Discussion

This study demonstrates the feasibility of fabricating hydrophobic surfaces through Digital Light Processing (DLP) by carefully controlling material selection, geometric texture, and surface modification. The observed differences in contact angles among the tested resins and textures emphasize the interplay between chemical composition and microstructure in dictating surface wettability. The intrinsic parameters, such as the polarity and functional groups of the resin matrix, directly affect surface energy, while extrinsic parameters—such as pillar shape, height, and spacing—govern the extent of air entrapment beneath a droplet. These factors determine whether the surface supports a Wenzel or Cassie–Baxter wetting regime, a distinction that critically influences hydrophobicity. Thus, the results not only validate the initial hypothesis but also provide mechanistic insight into how material and design choices enable tunable wetting states. The comparison between the three base resins reveals that resin chemistry has a direct and significant influence on surface wettability. Specifically, the Water-Washable resin exhibited the most hydrophobic behavior. This can be attributed to its unique chemical formulation, one which likely results in lower surface energy and more polar functional groups capable of reducing water adhesion. In contrast, the lower contact angles observed for TR300 and Speed may result from their different polymeric backbones and possibly involve more hydrophilic moieties or surface-active impurities. This highlights the importance of selecting resins not only based on their mechanical or printing properties, but also on their surface chemistry, when targeting water-repellent applications. The geometric configuration of surface textures played a central role in determining wetting behavior. Square-shaped microstructures outperformed cylindrical ones due to the sharp corners and flat sidewalls of the former, which more effectively trap air and sustain the Cassie–Baxter wetting regime. In contrast, the rounded curvature of cylindrical pillars facilitated greater liquid–solid contact, increasing the likelihood of Wenzel state transition. Theoretical models support this interpretation, highlighting the fact that texture shape, edge sharpness, and surface fraction determine the degree of air entrapment, which in turn governs hydrophobicity. This suggests that even with identical dimensions, square geometries offer an inherent mechanical advantage in repelling water, due to their anisotropic profiles. Feature width significantly influenced the wetting behavior of the textured surfaces. As the lateral dimensions of the square pillars increased, the available air volume and surface roughness also increased, improving the stability of the Cassie–Baxter state. For example, increasing the feature width of the

square pillars from $300 \times 300 \mu\text{m}$ to $460 \times 460 \mu\text{m}$ resulted in an increase in the apparent contact angle from $\sim 106^\circ$ to $\sim 128^\circ$, indicating improved air entrapment and enhanced Cassie–Baxter state stability. Similarly, for cylindrical textures, increasing the diameter from $200 \mu\text{m}$ to $300 \mu\text{m}$ raised the contact angle from $\sim 78^\circ$ to $\sim 100^\circ$, though square textures consistently outperformed cylindrical ones due to the sharper edges and flat sidewalls of the former. Wider features reduce the likelihood of liquid penetration into the grooves by enlarging the interfacial area in which air can remain trapped beneath the droplet. This creates a more robust composite solid–air interface, minimizing water–solid contact and enhancing apparent hydrophobicity. Thus, increasing this width strengthens the mechanical and thermodynamic stability of the hydrophobic regime. The height of the microstructured pillars critically affects the stability of the air layer trapped beneath the droplet, thereby influencing hydrophobicity. Taller pillars increase the vertical dimensions of air pockets, increasing the overall volume through which water cannot penetrate. This reduces the effective solid–liquid contact area and favors the Cassie–Baxter wetting regime, in which droplets rest on a composite surface of solid and air. As a result, the apparent contact angle increases, leading to more spherical droplets and decreased adhesion. Moreover, increased height can improve the mechanical robustness of the texture by providing better structural support to maintain the air layer during droplet impact or external stresses. The spacing between microstructured features significantly influences surface wettability by controlling the stability of trapped air pockets. Narrower spacing enhances air entrapment beneath droplets, minimizing direct water–solid contact and promoting a Cassie–Baxter wetting state with higher contact angles. Conversely, increased spacing allows water to infiltrate the texture, inducing a transition to the Wenzel state characterized by increased wettability and adhesion. Quantitatively, this transition manifests as a notable decrease in contact angle with wider spacing, observed consistently in both the square and cylindrical geometries. These findings align with established wetting theories that emphasize the critical role of texture spacing in maintaining the hydrophobic or superhydrophobic attributes of surfaces. Chemical surface modification using hydrophobic fluorosilane (HFS) significantly improves the wetting behavior by lowering surface energy and creating a uniform hydrophobic molecular layer. The treatment increased contact angles markedly from untreated values, with 1 wt.% HFS producing a substantial 32.9% enhancement in water repellency. Further increases in HFS concentration yielded smaller incremental gains, indicating saturation of reactive sites and formation of a near-complete monolayer. This plateau effect is consistent with surface adsorption models and highlights the fact that excessive chemical loading does not proportionally improve hydrophobicity. These findings emphasize that chemical functionalization synergizes with microstructural design to achieve optimal surface properties. Throughout this study, the term hydrophobicity refers specifically to static contact angle measurements, which were used to characterize surface wettability. While some of the trends—such as enhanced air entrapment—suggest a Cassie–Baxter wetting state, dynamic wetting properties (e.g., sliding angle or droplet mobility) were not measured, and remain outside the scope of this work.

In conclusion, the study demonstrates that a synergistic approach combining precise geometrical microstructuring, careful resin chemistry selection, and targeted surface chemical modification enables effective control over surface wettability in DLP-fabricated parts. This strategy provides a versatile and cost-effective route to engineer hydrophobic and superhydrophobic surfaces, with potential applications in biomedical devices, microfluidics, and anti-fouling coatings. Future research should focus on evaluating the mechanical robustness and environmental durability of these textures under real-world conditions, including abrasion resistance, chemical stability, and UV exposure. Furthermore, assessing their biofunctional performance, particularly bacterial adhesion inhibition and

biofilm prevention, will be crucial for validating their biomedical utility. The integration of multi-material printing and advanced post-processing techniques offers promising avenues to further optimize and diversify the functionality of such engineered surfaces across diverse sectors.

5. Conclusions

This study investigated the feasibility of fabricating hydrophobic surfaces using Digital Light Processing (DLP), through the design of surface geometries and the application of surface treatments. The primary goal was to evaluate the influence of resin selection, texture geometry, and hydrophobic surface coating on the wettability of 3D-printed polymer parts. The main findings can be summarized as follows:

1. The Water-Washable resin showed the highest contact angle (90.38°), representing a 26% increase compared to TR300 (71.77°), and a 15.4% increase compared to the Speed resin (78.3°). This highlights the critical role of intrinsic material properties in enhancing surface hydrophobicity.
2. Square microstructures outperformed cylindrical ones of the same size. For the $300\ \mu\text{m} \times 300\ \mu\text{m} \times 200\ \mu\text{m}$ design, the square pattern achieved a contact angle of 106.08° , compared to 99.62° for the cylindrical counterpart—a 6.5% increase due to improved air trapping and edge sharpness.
3. Increasing the square structure's width from $300\ \mu\text{m}$ to $460\ \mu\text{m}$ raised the contact angle from 106.08° to 128.36° , marking a 21% improvement in hydrophobicity due to better air retention.
4. Raising the pillar height from $350\ \mu\text{m}$ to $521\ \mu\text{m}$ resulted in a contact angle increase from 116.4° to 133.6° , corresponding to a 14.7% enhancement; this was attributed to the larger volume for air pockets and reduced solid–liquid contact.
5. In the square textures, increasing the spacing from $150\ \mu\text{m}$ to $258\ \mu\text{m}$ led to a drop in contact angle from 106.08° to 86.84° (18.1% decrease). Similarly, for cylindrical textures, the angle dropped from 99.6° to 69.6° (30.1% decrease), confirming that excessive spacing reduces hydrophobic performance by enabling the Wenzel state.
6. Applying 1 wt.% HFS coating raised the contact angle from 85.1° to 113.1° , representing a 32.9% increase. Further increases to 2 wt.% and 3 wt.% yielded 120.4° and 123.4° , respectively, indicating diminishing improvements beyond 1 wt.% due to surface saturation.

These results confirm that optimizing the geometry, resin selection, and surface treatment enables precise control over wettability in DLP-fabricated parts. This approach offers a low-cost, design-driven route to the manufacture of functional hydrophobic surfaces, with potential applications in biomedical devices, microfluidics, and self-cleaning materials. However, this study was limited to controlled laboratory conditions and short-term evaluations. Future studies should focus on the long-term durability of these hydrophobic surfaces under real-world conditions, such as abrasion, chemical exposure, and UV aging. Additionally, investigating antibacterial performance and biofilm resistance will be essential in assessing the suitability of these processes for biomedical and environmental applications.

Author Contributions: Conceptualization, M.B.; methodology, S.M.A.S. and M.B.; software, S.M.A.S.; validation, S.M.A.S., M.B. and B.A.; formal analysis, M.B. and S.M.A.S.; investigation, M.B. and S.M.A.S.; resources, M.B. and B.A.; data curation, M.B. and S.M.A.S.; writing—original draft preparation, S.M.A.S.; writing—review and editing, M.B.; supervision, M.B. and B.A.; project administration, M.B. and B.A. All authors have read and agreed to the published version of the manuscript.

Funding: This research received no external funding.

Data Availability Statement: The original contributions presented in this study are included in the article. Further inquiries can be directed to the corresponding author.

Conflicts of Interest: The authors declare no conflict of interest.

Abbreviations

The following abbreviations are used in this manuscript:

DLP	Digital Light Processing
SHB	Superhydrophobic
CAH	Contact Angle Hysteresis
TR300	A Type of Photopolymer Resin
Speed	A Type of Photopolymer Resin
HFS	Hydrophobic Fluoro-Silane
MSLA	Masked Stereolithography
RPM	Revolutions per Minute
VHX	A Type of Digital Microscope (KEYENCE VHX-5000)
µm	Micrometer
wt. %	Weight percent
UV	Ultraviolet

References

- Falde, E.J.; Yohe, S.T.; Colson, Y.L.; Grinstaff, M.W. Superhydrophobic Materials for Biomedical Applications. *Biomaterials* **2016**, *104*, 87–103. [CrossRef]
- Jeong, C. A Study on Functional Hydrophobic Stainless Steel 316L Using Single-Step Anodization and a Self-Assembled Monolayer Coating to Improve Corrosion Resistance. *Coatings* **2022**, *12*, 395. [CrossRef]
- Bai, M.; Kazi, H.; Zhang, X.; Liu, J.; Hussain, T. Robust Hydrophobic Surfaces from Suspension HVOF Thermal Sprayed Rare-Earth Oxide Ceramics Coatings. *Sci. Rep.* **2018**, *8*, 6973. [CrossRef]
- Farzam, M.; Beitollahpoor, M.; Solomon, S.E.; Ashbaugh, H.S.; Pesika, N.S. Advances in the Fabrication and Characterization of Superhydrophobic Surfaces Inspired by the Lotus Leaf. *Biomimetics* **2022**, *7*, 196. [CrossRef]
- Antonov, D.V.; Islamova, A.G.; Strizhak, P.A. Hydrophilic and Hydrophobic Surfaces: Features of Interaction with Liquid Drops. *Materials* **2023**, *16*, 5932. [CrossRef]
- Jokinen, V.; Kankuri, E.; Hoshian, S.; Franssila, S.; Ras, R.H.A. Superhydrophobic Blood-Repellent Surfaces. *Adv. Mater.* **2018**, *30*, 1705104. [CrossRef] [PubMed]
- Liu, H.; Zhang, Z.; Wu, C.; Su, K.; Kan, X. Biomimetic Superhydrophobic Materials through 3D Printing: Progress and Challenges. *Micromachines* **2023**, *14*, 1216. [CrossRef]
- Young, B.R.; Pitt, W.G.; Cooper, S.L. Protein Adsorption on Polymeric Biomaterials: II. Adsorption Kinetics. *J. Colloid Interface Sci.* **1988**, *125*, 246–260. [CrossRef]
- Schmidt, D.R.; Waldeck, H.; Kao, W.J. Protein Adsorption to Biomaterials. In *Biological Interactions on Materials Surfaces: Understanding and Controlling Protein, Cell, and Tissue Responses*; Puleo, D.A., Bizios, R., Eds.; Springer: New York, NY, USA, 2009; pp. 1–18, ISBN 978-0-387-98161-1.
- Non-Fouling Surfaces—Buddy Ratner Biomaterials Group. Available online: https://sites.uw.edu/biomaterialsgroup/research/non-fouling-surfaces/?utm_source=chatgpt.com (accessed on 5 February 2025).
- Ballester-Beltrán, J.; Rico, P.; Moratal, D.; Song, W.; Mano, J.F.; Salmerón-Sánchez, M. Role of Superhydrophobicity in the Biological Activity of Fibronectin at the Cell–Material Interface. *Soft Matter* **2011**, *7*, 10803. [CrossRef]
- Shadpour, H.; Sims, C.E.; Thresher, R.J.; Allbritton, N.L. Sorting and Expansion of Murine Embryonic Stem Cell Colonies Using Micropallet Arrays. *Cytometry A* **2009**, *75A*, 121–129. [CrossRef] [PubMed]
- Shen, J.; Gao, P.; Han, S.; Kao, R.Y.T.; Wu, S.; Liu, X.; Qian, S.; Chu, P.K.; Cheung, K.M.C.; Yeung, K.W.K. A Tailored Positively-Charged Hydrophobic Surface Reduces the Risk of Implant Associated Infections. *Acta Biomater.* **2020**, *114*, 421–430. [CrossRef]
- Kang, J.-W.; Jeon, J.; Lee, J.-Y.; Jeon, J.-H.; Hong, J. Surface-Wetting Characteristics of DLP-Based 3D Printing Outcomes under Various Printing Conditions for Microfluidic Device Fabrication. *Micromachines* **2023**, *15*, 61. [CrossRef]
- Rodič, P.; Kovač, N.; Kralj, S.; Jereb, S.; Golobič, I.; Može, M.; Milošev, I. Anti-Corrosion and Anti-Icing Properties of Superhydrophobic Laser-Textured Aluminum Surfaces. *Surf. Coat. Technol.* **2024**, *494*, 131325. [CrossRef]
- A., K.S.; P., D.; G., D.; J., N.; G.S., H.; S., A.S.; K., J.; R., M. Super-Hydrophobicity: Mechanism, Fabrication and Its Application in Medical Implants to Prevent Biomaterial Associated Infections. *J. Ind. Eng. Chem.* **2020**, *92*, 1–17. [CrossRef]

17. Zhang, Y.; Zhang, Z.; Yang, J.; Yue, Y.; Zhang, H. A Review of Recent Advances in Superhydrophobic Surfaces and Their Applications in Drag Reduction and Heat Transfer. *Nanomaterials* **2021**, *12*, 44. [CrossRef]
18. Barthlott, W.; Neinhuis, C. Purity of the Sacred Lotus, or Escape from Contamination in Biological Surfaces. *Planta* **1997**, *202*, 1–8. [CrossRef]
19. Atwah, A.A.; Almutairi, M.D.; He, F.; Khan, M.A. Influence of Printing Parameters on Self-Cleaning Properties of 3D Printed Polymeric Fabrics. *Polymers* **2022**, *14*, 3128. [CrossRef] [PubMed]
20. Fan, S.; Jiang, S.; Wang, Z.; Liang, P.; Fan, W.; Zhuo, K.; Xu, G. Fabrication of Durable Superhydrophobic Surface for Versatile Oil/Water Separation Based on HDTMS Modified PPy/ZnO. *Nanomaterials* **2022**, *12*, 2510. [CrossRef] [PubMed]
21. Kaur, G.; Marmur, A.; Magdassi, S. Fabrication of Superhydrophobic 3D Objects by Digital Light Processing. *Addit. Manuf.* **2020**, *36*, 101669. [CrossRef]
22. Efremov, A.N.; Stanganello, E.; Welle, A.; Scholpp, S.; Levkin, P.A. Micropatterned Superhydrophobic Structures for the Simultaneous Culture of Multiple Cell Types and the Study of Cell-Cell Communication. *Biomaterials* **2013**, *34*, 1757–1763. [CrossRef]
23. Duda, T.; Raghavan, L.V. 3D Metal Printing Technology. *IFAC-Pap.* **2016**, *49*, 103–110. [CrossRef]
24. Chaudhary, R.; Fabbri, P.; Leoni, E.; Mazzanti, F.; Akbari, R.; Antonini, C. Additive Manufacturing by Digital Light Processing: A Review. *Prog. Addit. Manuf.* **2023**, *8*, 331–351. [CrossRef]
25. Ford, S.; Despeisse, M. Additive Manufacturing and Sustainability: An Exploratory Study of the Advantages and Challenges. *J. Clean. Prod.* **2016**, *137*, 1573–1587. [CrossRef]
26. Srivastava, M.; Rathee, S. Additive Manufacturing: Recent Trends, Applications and Future Outlooks. *Prog. Addit. Manuf.* **2022**, *7*, 261–287. [CrossRef]
27. Gibson, I.; Rosen, D.; Stucker, B.; Khorasani, M. *Additive Manufacturing Technologies*; Springer International Publishing: Cham, Switzerland, 2021; ISBN 978-3-030-56126-0.
28. Han, Y.; Liu, Y.; Kaneko, M.; Uchikoba, F. Profile Characterization and Temperature Effect on the Wettability of Microstructured Surfaces. *J. Surf. Eng. Mater. Adv. Technol.* **2018**, *8*, 83–94. [CrossRef]
29. Tadmor, R.; Das, R.; Gulec, S.; Liu, J.; N’guessan, H.E.; Shah, M.; Wasnik, P.S.; Yadav, S.B. Solid–Liquid Work of Adhesion. *Langmuir* **2017**, *33*, 3594–3600. [CrossRef]
30. Liu, M.; Wang, S.; Wei, Z.; Song, Y.; Jiang, L. Bioinspired Design of a Superoleophobic and Low Adhesive Water/Solid Interface. *Adv. Mater.* **2009**, *21*, 665–669. [CrossRef]
31. Feng, L.; Li, S.; Li, Y.; Li, H.; Zhang, L.; Zhai, J.; Song, Y.; Liu, B.; Jiang, L.; Zhu, D. Super-Hydrophobic Surfaces: From Natural to Artificial. *Adv. Mater.* **2002**, *14*, 1857–1860. [CrossRef]
32. Wenzel, R.N. Resistance of Solid Surfaces to Wetting by Water. *Ind. Eng. Chem.* **1936**, *28*, 988–994. [CrossRef]
33. Wang, J.; Do-Quang, M.; Cannon, J.J.; Yue, F.; Suzuki, Y.; Amberg, G.; Shiomi, J. Surface Structure Determines Dynamic Wetting. *Sci. Rep.* **2015**, *5*, 8474. [CrossRef]
34. Hashim, J.; Looney, L.; Hashmi, M.S.J. The Wettability of SiC Particles by Molten Aluminium Alloy. *J. Mater. Process. Technol.* **2001**, *119*, 324–328. [CrossRef]
35. Zhang, T.; Wang, J.; Chen, L.; Zhai, J.; Song, Y.; Jiang, L. High-Temperature Wetting Transition on Micro- and Nanostructured Surfaces. *Angew. Chem. Int. Ed.* **2011**, *50*, 5311–5314. [CrossRef] [PubMed]
36. Young, T. III. An Essay on the Cohesion of Fluids. *Philos. Trans. R. Soc. Lond.* **1805**, *95*, 65–87. [CrossRef]
37. Cassie, A.B.D.; Baxter, S. Wettability of Porous Surfaces. *Trans. Faraday Soc.* **1944**, *40*, 546–551. [CrossRef]
38. Drelich, J.W.; Boinovich, L.; Chibowski, E.; Della Volpe, C.; Hołysz, L.; Marmur, A.; Siboni, S. Contact Angles: History of over 200 Years of Open Questions. *Surf. Innov.* **2020**, *8*, 3–27. [CrossRef]
39. TR300 Ultra-High Temp 3D Printing Resin. Available online: <https://phrozen3d.com/products/tr300-ultra-high-temp-resin> (accessed on 15 February 2025).
40. Phrozen Speed 3D Printing Resin. Available online: <https://phrozen3d.com/products/speed-resin> (accessed on 15 February 2025).
41. Phrozen Water-Washable Dental Model Resin. Available online: <https://3dpartnershop.com> (accessed on 14 August 2025).

Disclaimer/Publisher’s Note: The statements, opinions and data contained in all publications are solely those of the individual author(s) and contributor(s) and not of MDPI and/or the editor(s). MDPI and/or the editor(s) disclaim responsibility for any injury to people or property resulting from any ideas, methods, instructions or products referred to in the content.